The Influence of Bubbles on Ambient Noise in the Ocean at High Wind Speeds

DAVID M. FARMER

Institute of Ocean Sciences, Sidney, B.C. V8L 4B2, Canada

DAVID D. LEMON

Arctic Sciences Ltd., Sidney, B.C. V8L 3S1, Canada

(Manuscript received 29 February 1984, in final form 9 July 1984)

ABSTRACT

Observations of ambient noise in the ocean at high wind speeds reveal significant departures in spectral shape from previously reported values at lower wind speeds. The observations were made in open ocean conditions in Queen Charlotte Sound, British Columbia, in bands centered at frequencies of 4.3, 8.0, 14.5 and 25.0 kHz; surface wind speeds up to 25 m s^{-1} were recorded. Ambient noise at 4.3 kHz displayed a logarithmic relationship with wind speed throughout the observed speed range, similar to that reported previously. However, at the two higher frequencies (14.5 and 25.0 kHz), the noise spectrum levels did not increase with increasing wind speed at the same rate and for winds above about 15 m s^{-1} the noise levels actually decreased with increasing wind speed. Similar though less extreme behavior was observed at 8.0 kHz. We attribute this effect to the presence of bubbles which are known to be entrained at the surface of the ocean. The hypothesis is explored with a model in which the noise source is assumed uniformly distributed over the surface and the sound is both scattered and absorbed by a thin layer of bubbles. Inferred bubble population densities are found to be consistent with previous estimates based on photographic observations. However the wide range of wind speeds encountered allows us to derive a more complete relationship between population density and wind speed and the use of different frequencies provides information on the bubble size distribution. The attenuating effect of bubbles has implications for the use of ambient noise for remote sensing of processes at the air–sea interface.

1. Introduction

From the earliest studies of ambient noise in the ocean it has been apparent that the action of wind on the sea surface constitutes an important natural source of sound, often dominating all others over a broad range of frequencies (Knudsen *et al.*, 1948). Physical mechanisms proposed for its generation include nonlinear wave interactions (5–10 Hz), turbulent pressure fluctuations in the atmosphere over the ocean (10–80 Hz) and at higher frequencies the impact of ocean spray, oscillating bubbles, cavitation noise and the interaction of turbulent flows with entrained air in breaking waves (cf. Wenz, 1962; Wilson, 1980; Kerman, 1984).

The close relationship between wind speed and noise level provides the basis for an effective remote sensing scheme in which wind speed may be derived from recorded ambient noise using empirically determined calibrations (Shaw *et al.*, 1978). More recently it has been shown that ambient noise measurements can also provide the basis for inferring precipitation (Lemon *et al.*, 1984). From an oceanographic point of view, the measurement of relatively infrequent high wind speeds is of great importance since the stress of the wind on the ocean surface is approximately proportional to the square of the wind speed and the rate at which the wind does work on the surface depends on the product of wind speed and stress. Thus occasional intense storms can have an influence on the momentum balance and surface density structure out of all proportion to their frequency and duration. However, while measurements of ambient noise are extensive, there are few published accounts of observations at the higher wind speeds (>12 m s^{-1}) which are also of interest to oceanographers, especially at higher acoustic frequencies (>10 kHz). The present study is concerned with ambient noise at frequencies up to 25 kHz and wind speeds up to 25 m s^{-1}.

The observations reveal a significant modification in the spectral properties of the noise at wind speeds >10 m s^{-1}, especially at the higher acoustic frequencies (14.5 and 25.0 kHz). For sufficiently high wind speeds an increase in wind speed results in a decrease in noise level. We examine the hypothesis that this change in spectral shape is caused not by any alteration in the noise generating mechanism, but rather by the thin layer of entrained bubbles that is known to occur near the surface of the ocean and serves both to

absorb and scatter the sound originating at the air–sea interface. On the basis of this hypothesis, the apparent attenuation of the ambient noise serves as a probe with which to determine the properties and behavior of the bubble layer itself.

2. Observations

The observations described here were taken during the winter of 1982/83 in open-ocean conditions near the shelf break of Queen Charlotte Sound (Fig. 1). The instrument type (Sea Data Model 661, see Hill, 1984) and locations were almost identical to those used during an earlier experiment (Lemon *et al.*, 1984), although the operating frequency of one channel of one instrument was increased to 25 kHz (see Table 1). The data were sampled in 112.5 s segments each of which was recorded on magnetic tape. The earlier experiment, described by Lemon *et al.* (1984), was limited to wind speeds of less than 12 m s^{-1} and demonstrated a relationship between ambient noise and wind speeds measured from moored anemometers in rather close agreement with previous observations in the deep ocean.

Our redeployment of the instruments in October 1982 coincided with the installation of a wave height recording buoy near to our southern mooring (Fig.

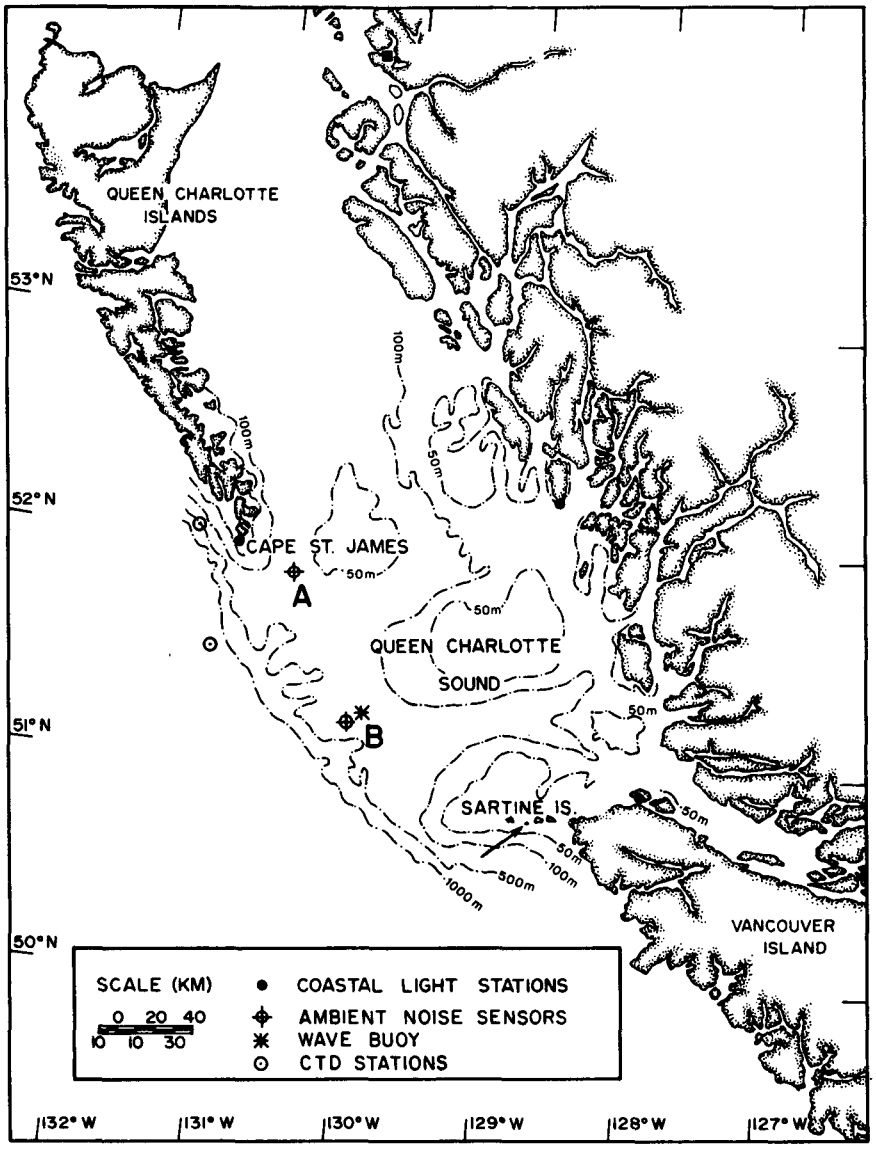

FIG. 1. Map showing location of recording instruments at Stations A and B on the continental shelf off Canada's west coast. A wave height recorder was moored close to Station B. The Cape St. James lightstation north of Station A provided wind and precipitation data. CTD stations just west of the shelf break near Station A provide representative sound speed profiles.

TABLE 1. Deployment information for ambient noise measurements.

	Location	
	A	B
Depth (m)	267	253
Frequencies (KHz)	4.3, 14.5, 25.0	4.3, 8.0, 14.5
Deployment period	19 October 1982–27 January 1983	15 October 1982–31 January 1983
Sampling period	112.5 s	112.5 s

1) as part of an independent study. As in the earlier summer deployment, two surface moorings with Aanderaa anemometers at 3 m height were placed near each of the ambient noise recorders. Unfortunately one of these was lost during the winter and the other severely damaged, so that only a small section of wind record from the southern instrument survived. For this reason, quite apart from the other limitations of anemometry from surface moorings in high winds, our comparisons between ambient noise and local wind speed are based on two land stations, Sartine Island and the Cape St. James lighthouse. Both of these are on very exposed locations, the Cape St. James station being 20 km north of our northern mooring and Sartine Island 150 km south of our southern instrument. However in contrast to ambient noise comparisons with the moored anemometer measurements made during the summer, and as might be expected given the geographical separation, wind measurements from the lightstations are less well correlated with the ambient noise, especially at low wind speeds. Nevertheless, above 12 m s^{-1}, the Cape St. James data follow the same trend as the surface-moored anemometer data, as shown in Fig. 2. A least-squares fit of the Cape St. James lightstation data to the 4.3-kHz noise spectrum level (NSL) from Station A for speeds greater than 5 m s^{-1} yields a relationship with almost identical slope to that derived from the wind speed measurements obtained by the Aanderaa anemometer at 3 m height during the previous summer. In determining these relationships recorded wind speeds above and below 5 m s^{-1} were treated separately since a change in wind speed dependence has been noted at this value due to the onset of whitecapping (Evans and Watts, 1982; Kerman *et al.*, 1983). The noise levels in Fig. 2 and subsequently in this paper are expressed as dB re 1 μPa^2 Hz^{-1}.

Queen Charlotte Sound is frequently swept by strong winds in autumn and winter. A warm surface layer develops during summer, but wind mixing and convection later in the year can erode the stratification leaving almost isothermal conditions throughout the winter. No hydrographic observations are available immediately adjacent to the deployment sites during the experiment, but salinity and temperature data (Fig. 3) from stations just west of the shelf provide profiles of the local water mass which will be representative of conditions on the shelf, especially at Station A. These show the water to be well mixed down to about 100 m, with relatively minor variations in sound speed. For the profile drawn we have also calculated refracted ray paths applicable between the surface and 267 m, which is the depth of the hydrophone at Station A (see Fig. 4a). For paths meeting the surface at a radius less than about 6 km, refractive effects are minor, and the sound paths deviate only slightly from straight lines. This allows a simplification in our subsequent analysis of measurements at the two higher frequencies for which absorption is substantial over these ranges. The significance of absorption is illustrated in Fig. 4b, where we have plotted that fraction of the total unreflected sound (reaching the hydrophone) that is generated at the ocean surface within a circle of given radius centered over the measurement site. The calculation assumes a horizontally homogeneous dipole source pattern and uses constant absorption coefficients for each frequency appropriate to the local temperature field, as listed in Table 2. At 14.5 and 25.0 kHz, most of the received signal comes from within a circle of 6 km, thus justifying our neglect of refractive effects at these frequencies. At the lower frequencies, for which the absorption coefficient is smaller, this simplification might not apply. As discussed subsequently, the contribution from multiple reflections is minor and can be safely neglected in the present study.

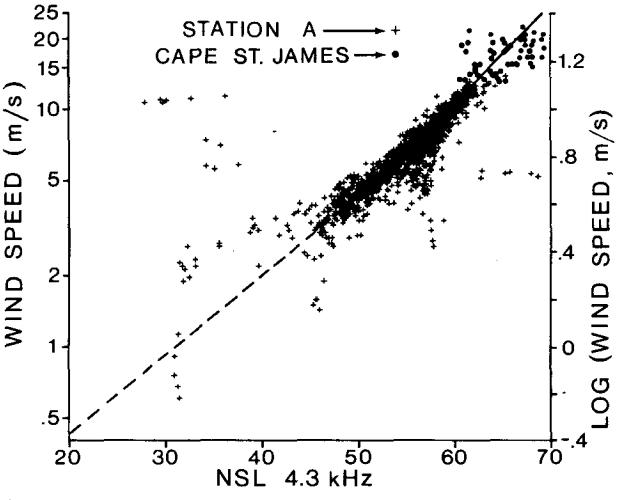

FIG. 2. Plot of wind speed against noise spectrum levels recorded at 4.3 kHz at Station A including both summer data taken with an Aanderaa anemometer at Station A and, for wind speeds greater than 12 m s^{-1}, winter data derived from Cape St. James lightstation. Straight lines are drawn based on least-squares fits between the summer data from the moored anemometer and 4.3 kHz NSL at Station A. Solid lines: wind speeds (W) for $W > 5$ m s^{-1}. Dashed lines: $W < 5$ m s^{-1}. Noise spectrum level (NSL) is expressed in dB re 1 μPa^2 Hz^{-1}.

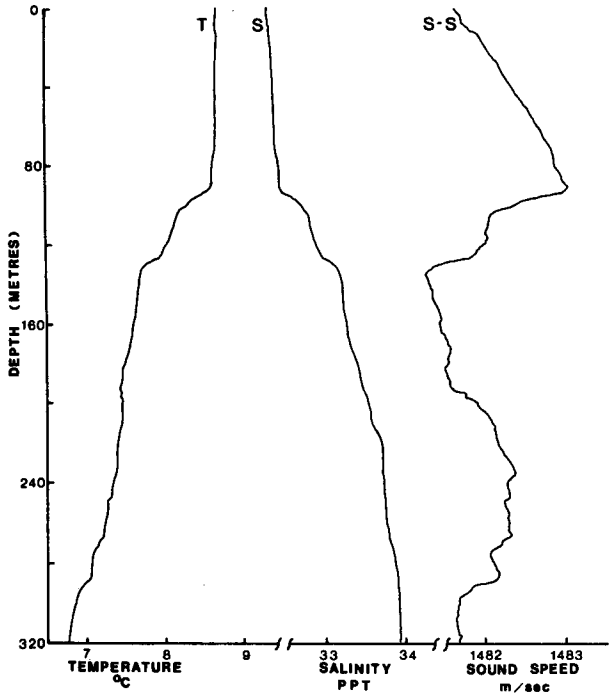

FIG. 3. Profiles of salinity, temperature and sound speed, on 2, December 1982 just beyond the shelf-break, west of Station A.

Over the frequency range of interest (4.3–25.0 kHz), contributions to the ambient noise also arise from shipping and from precipitation. Noise from ships appears as occasional peaks in the time series with low frequencies predominating and is fairly easily identified, but precipitation noise occurs over longer periods and includes significant higher-frequency components. One purpose of the earlier experiment was the detection of noise due to precipitation and the exploration of its potential as a remote sensing signal. For reasons that will become apparent in the present study, a simple extrapolation of results from low to high wind speeds will not be appropriate and the precipitation-induced noise under these conditions will not be treated here. The present discussion is concerned with measurements made during periods for which no significant precipitation was recorded at the two lightstations. Nevertheless there is some evidence in the data that rain did occasionally fall near the instruments during these periods and contribute to the recorded noise.

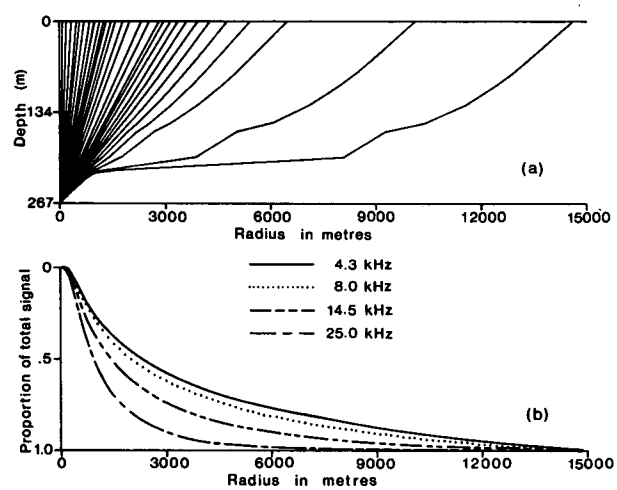

FIG. 4. (a) Refracted sound paths calculated for the upper 267 m of the sound speed profile shown in Fig. 3, applicable to Station A. Sound paths reaching a hydrophone on the sea floor from points on the ocean surface within a radius of about 6 km are only weakly refracted. (b) Curves showing that fraction of unreflected sound generated at the sea surface reaching the hydrophone at Station A, originating from within a circle of given radius. The calculation is for direct paths only and assumes a horizontally uniform source with a dipole radiation pattern. Attenuation is calculated assuming absorption by the water given by coefficients in Table 3, applicable at 8°C.

3. Results

a. Wind wave—ambient noise relations

During the winter several intense atmospheric disturbances moved through Queen Charlotte Sound. Maximum wind speeds of 30 m s^{-1} were recorded at the lightstations. Some of these events passed without recorded precipitation at the nearby lightstations and were thus selected for the present study. During these storms the strong winds were generally from west or south so that there was essentially unrestricted fetch. For each 20-minute set of wave measurements observed with the wave height recorder, a "maximum significant wave height" is computed, approximately equal to the mean of the higher one-third of observed wave heights. Individual waves are likely to exceed this value by up to 30%. During storms, maximum significant wave heights of 12 m were reached.

Figure 5a shows a short time series of 14.5 and 4.3 kHz signals, converted to wind speed using the calibration factors found for the same location (Station B) the previous summer. At lower wind speeds ($W < 12$ m s^{-1}) the two records are almost identical, but at higher wind speeds the 14.5 kHz record does not correspond so well, appearing to be "clipped", as though the signal were suppressed. This cannot be attributed to saturation of the electronics, since the

TABLE 2. Bubble damping constant δ, scattering cross-section σ_s and absorption cross section σ_a for resonant bubbles at a depth of 1 m. Absorption coefficient α for sea water at 8°C.

Frequency (KHz)	δ	σ_s (cm^2)	σ_a (cm^2)	α (m^{-1})
4.3	0.0402	48.90	93.23	3.45×10^{-5}
8.0	0.0486	9.52	24.03	1.19×10^{-4}
14.5	0.0590	1.94	6.37	3.93×10^{-4}
25.0	0.0708	0.45	1.85	11.70×10^{-4}

signal falls well within the observable dynamic range. Plots of time series derived from channels tuned to the higher frequency (25 kHz) at Station A show similar behavior with the effect even more noticeable (see Fig. 5b). At higher wind speeds the 25 kHz signal actually decreases as the 4.3 kHz signal increases. Figure 5b also shows corresponding air and water

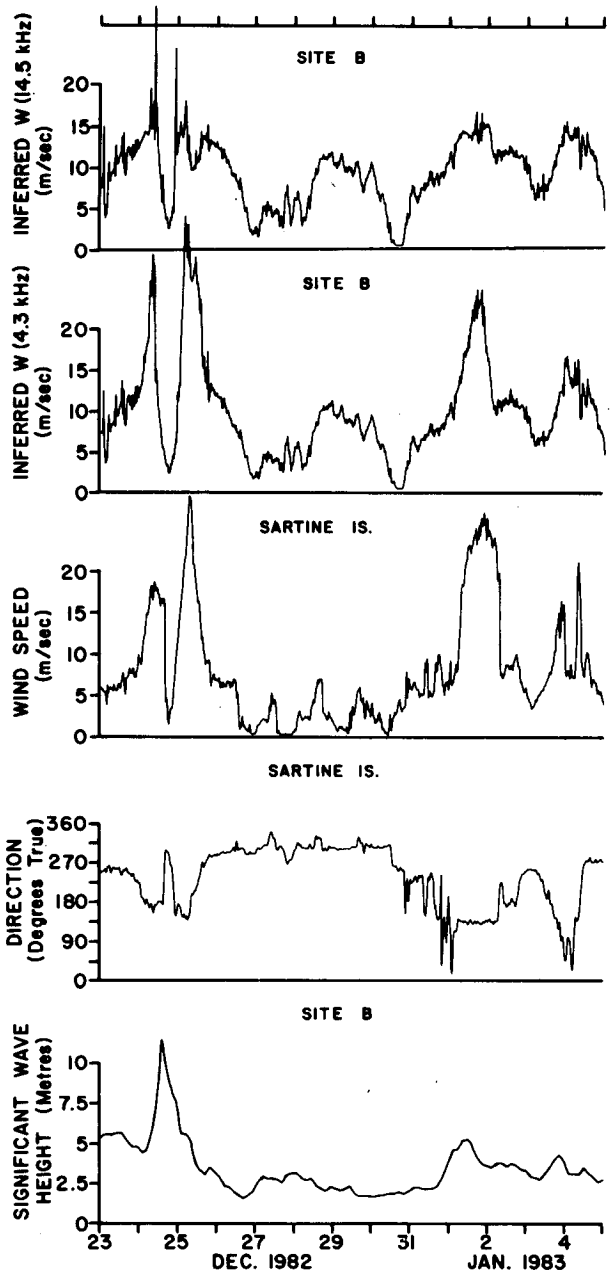

FIG. 5a. Time series plots of inferred wind speed at Station B based on NSL at 14.5 and 4.3 kHz, together with observed wind speed and direction at Sartine Island and significant wave height. Although inferred wind speeds are consistent between the two frequency channels below 10 m s^{-1}, at higher wind speeds the 14.5-kHz signal consistently understates the observed wind.

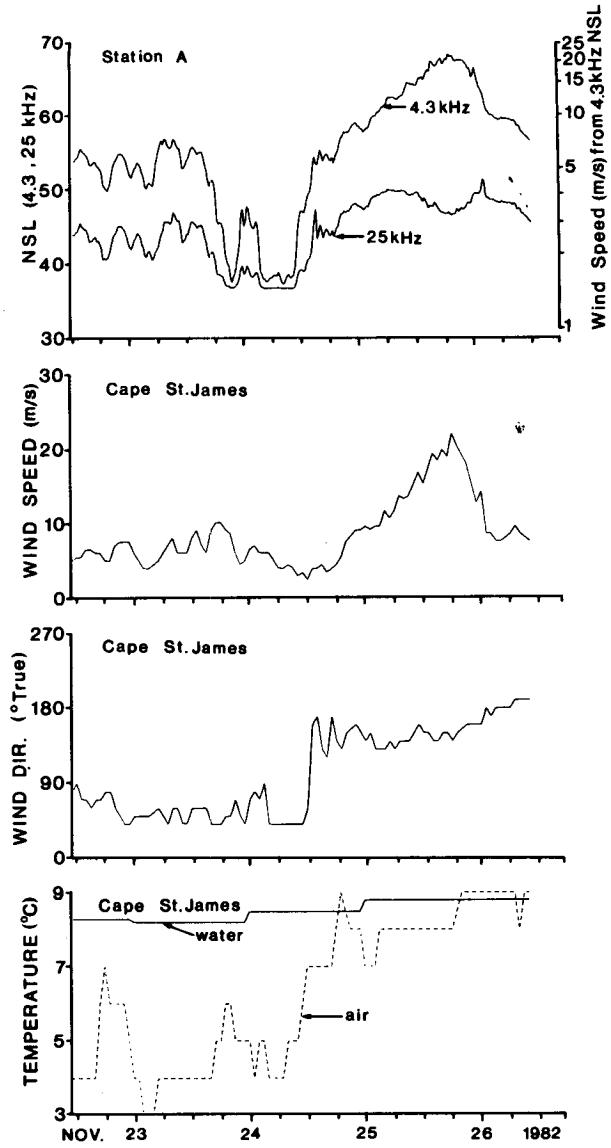

FIG. 5b. Noise spectrum level at 4.3 kHz and 25.0 kHz at Station A, together with wind speed and direction and air and sea surface temperatures at Cape St. James. The time series, identified as Series 3, was devoid of recorded rainfall and was thus selected for further analysis.

temperatures at the Cape St. James lighthouse. For the first part of the record air temperatures were appreciably lower than water temperatures, but for the latter portion, which includes the period of high wind speeds of special interest in this study, the temperature difference almost disappeared. Neutral stability is assumed for friction velocity estimates calculated for this period, which is also the period used for the subsequent frequency analysis. We refer subsequently to this data set as Series 3, since it corresponds to the third storm recorded during the winter measurements. We note that for the period of

strong winds during this storm, the wind direction was from the south, so that the fetch was essentially unrestricted.

The Sartine Island anemometer record follows the general pattern of the storms recorded at Station B, (see Fig. 5a), but differs in detail as might be expected given the distance between the two locations. For the storm that passed through the area on 24/25 December, the marked double peak apparent in the wind speed is not reproduced in the wave height measurements. This is not inconsistent with other wave observations which typically show the influence of winds well removed from the observation site, as well as the time lag associated with the growth of waves and the complicating effects of variable wind direction. In his analysis of the relationship between wind, wave heights and ambient noise up to 2.8 kHz, Perrone (1969) showed that cross-correlation maxima between wind and ambient noise occurred at zero lag, but those between ambient noise and wave height and between wind speed and wave height occur with a phase lag of several hours with the wave height fluctuation following the wind and ambient noise fluctuations. While there is considerable variability in the data sets obtained from Queen Charlotte Sound, in every case the lag in cross-correlation maxima between ambient noise and wave height has the same sign as that found by Perrone. Figure 6 shows the results of the correlation calculation carried out on the data for Series 3. The maximum correlation tends to be slightly lower and the lag tends to be slightly greater at higher acoustic frequencies, an effect that must partly arise from the influence of bubbles to be discussed; there is also a noticeable flattening of the correlation function at the origin, suggesting that at least part of the noise can be identified with wave height rather than wind speed. However, the dominant component of ambient noise in this frequency range is more closely related to the local wind speed than to wave heights and thus confirms and extends Perrone's results by nearly a decade in frequency.

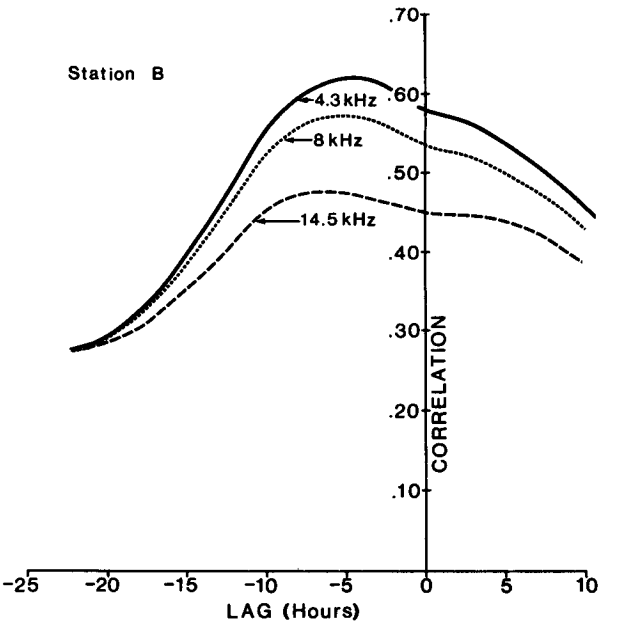

FIG. 6. Cross-correlations between noise spectrum levels (NSL) and significant wave height recorded at Station B. Negative values correspond to the significant wave height signal lagging the NSL time series. Maximum correlation occurs with the wave height signal following the noise spectrum levels by 5–6 h. A noticeable flattening of the correlation function occurs at the origin.

b. Ambient noise—spectral relationships

The most interesting relationships derived from the present study are those between signals recorded at different frequencies. If the noise generated by wind action on the ocean surface over some frequency band results from a self-similar process, we anticipate that it will exhibit a constant spectral slope independent of wind speed. That the spectral slope is indeed constant over a wide frequency range appears to be supported by many studies (e.g., see Wenz, 1962) and the "Knudsen spectra" are accepted as representative of wind generated noise, with a slope of −17 dB/decade between 500 and 50 000 Hz. More recently several measurements of ambient noise over limited segments of this frequency band (<2.4 kHz) have confirmed the general shape of the spectra, although certain variations are observed as a function of depth, frequency and wind speed (Perrone, 1969, 1970). At higher frequencies, spectral slope measurements are sparse. McConnell (1983) reports a spectral plateau in the range 15–20 kHz. Evans and Watts (1981) estimated slopes within ±2 dB of −17 dB/decade over the range 4.3–14.5 kHz. Scatter plots of noise levels at one frequency against those at another consistently yield straight lines for wind speeds up to 10 m s^{-1}. Departures from linearity can occur at low wind speeds (<2 m s^{-1}), especially at higher frequencies, on account of biological or other site-dependent effects (see Lemon *et al.*, 1984). Observations at frequencies above 5 kHz for wind speeds greater than 10 m s^{-1} are generally lacking, although Wille and Geyer (1984) have recently described measurements in relatively shallow water of the North and Baltic Seas (~30 m) which illustrate some of the features analyzed here, including a change in sign of the wind speed dependence at high frequencies. The ambient noise levels at these higher speeds and frequencies are the focus of the present study; departures from linearity in the respective frequency relationships constitute the appropriate signal for analysis.

Figure 7a shows recorded noise-spectrum levels (NSL) at 8.0 and 14.5 kHz for Station B, and Fig. 7b shows corresponding NSL for 14.5 and 25.0 kHz for Station A, Series 3, plotted against the corresponding 4.3-kHz values, together with wind speeds inferred

from anemometer calibrations as discussed before. Each plot is derived from 3072 NSL pairs. Except at the highest wind speeds the 8.0 versus 4.3 kHz plot is remarkably linear, consistent with a constant spectral slope over this frequency range. Departure from this linear relationship is more obvious at higher frequencies; at 14.5 and 25.0 kHz the slope of the curve changes sign at sufficiently high wind speeds. At low wind speeds the points also depart from a linear relationship at Station A and to a much smaller extent at Station B. The origin of this site-dependent effect at low wind speeds, which was also observed in the summer data (see Lemon *et al.*, 1984) is undetermined, but it is too small to affect the observations at higher speeds; at speeds above 4 m s^{-1}, scatter plots of the two 14.5 versus 4.3 kHz signals from each station were essentially identical.

The change in spectral slope with wind speed is even more clearly illustrated in Fig. 7c, which shows a plot of 25.0 kHz against 14.5 kHz noise spectrum levels. Except at low wind speeds, points corresponding to NSL less than 50 dB at 25.0 kHz and less than 52.5 dB at 14.5 kHz, fall close to a line of unit slope corresponding to a mean spectral roll-off of −16.8 dB/decade, independent of wind speed. At wind speeds greater than approximately 13 m s^{-1}, corresponding to NSL of 63 dB at 4.3 kHz, the points lie close to a line of slope −2 and the spectral slope is a sensitive function of wind speed.

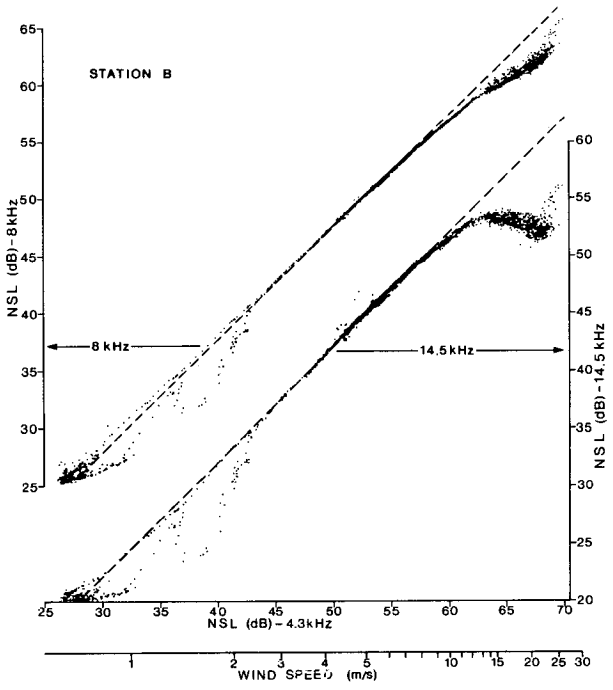

FIG. 7a. NSL plots for 8.0 and 14.5 kHz against 4.3 kHz at Station B. If the spectral slope over the plotted frequency intervals is independent of wind speed, the points should lie on a straight line of unit slope. Dashed line of unit slope demonstrates the extent to which the independence with respect to wind speed holds. Departures at low wind speed appear to be due to contamination by ship traffic noise; at high wind speed departure from linearity is attributed to bubbles.

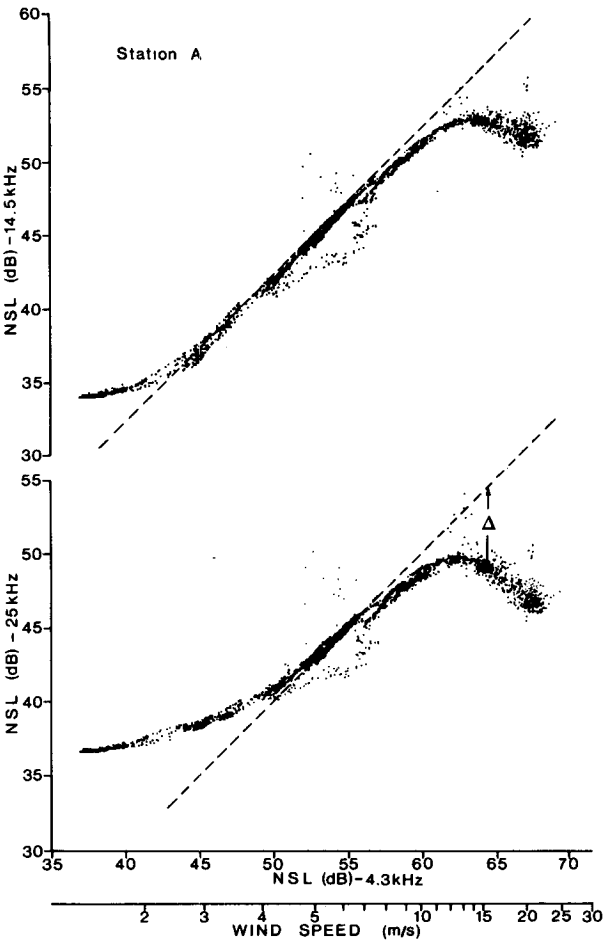

FIG. 7b. As for (a) but for Station A, 25.0 and 14.5 kHz NSL plotted against 4.3 kHz NSL. Departure from linearity at low wind speed is due to a site-dependent source of unknown origin. Departures from linearity at high wind speed, indicated by Δ, form the signal analyzed for bubble effects.

Although wind speeds during the storm of 22–26 November were not so great as during some other storms in the time series, this period is selected for analysis because the data set appears to be relatively free of contamination. For comparison a plot of 25.0 versus 4.3 kHz data from a subsequent storm (Series 4) is shown in Fig. 8. We interpret scatter from the principal curve as having arisen from two sources. Points lying above the curve represent signals containing a greater proportion of higher-frequency components. These are to be expected in the presence of rainfall; for periods in which significant rainfall was recorded at the lighthouse stations, many points lie above the curve. The second source of scatter appears to arise from local ship traffic. Unless a vessel passes very close, lower frequencies predominate; thus con-

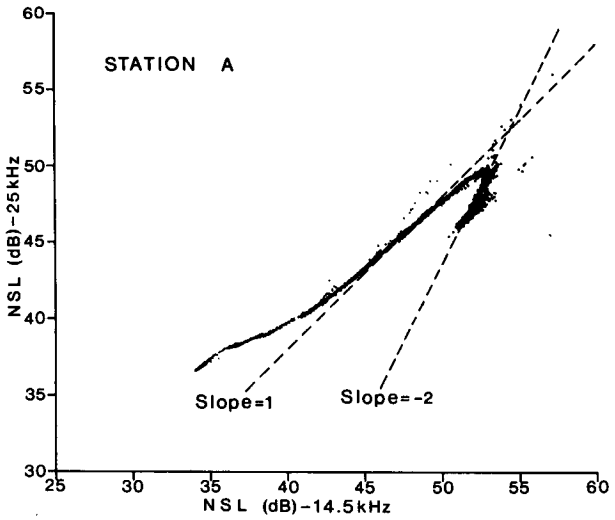

FIG. 7c. Plot of 25.0 against 14.5 kHz NSL for Station A. At high wind speeds both channels show a reduction in NSL with increasing speed. We have used the convention of a negative slope to represent this effect.

tamination by ship noise leads to a series of points lying below the curve, typically in a coherent pattern formed as the vessel range gradually changes.

At intermediate wind speeds the frequency plots display a banded structure. This feature is present to some extent on plots derived from all of the storms analyzed and appears to be associated with transient adjustments in spectral slope to changing wind and wave conditions.

4. Discussion

a. Scattering and absorption of sound by bubbles

Our observations of ambient noise over the frequency range 4.3–25.0 kHz demonstrate that the spectral slope is not independent of wind speed for $W > 10$ m s^{-1}. Instead the noise at 14.5 kHz and 25 kHz reaching our instruments not only ceases to increase but actually starts to decrease with increasing wind speed above a certain level.

We do not yet have a complete model of the noise-generating process, but the mechanisms considered thus far could hardly be expected to cause a decrease in noise with increasing wind speed. An alternative explanation is that the sound generated at the sea surface is attenuated in the surface zone and that this attenuation increases both with wind speed and with frequency. We anticipate that the cause of this attenuation will be the presence of air entrained into the surface layer by breaking waves.

There have been relatively few direct observations of bubbles near the surface of the ocean. Direct measurements of bubbles most relevant to wind generation, rather than biological production, are the photographic observations of Johnson and Cooke (1979) and the bubble trap observations of Kolovayev (1976) (see Wu, 1981). The bubble population density n, appears to depend on the bubble radius a as $n(a) \propto a^{-p}$ with $3.5 < p < 5$; the population density decreases exponentially with depth, with an e-folding scale of order 1 m which depends on the wind speed. Johnson and Cooke (1979) report a 20-fold increase in bubble population between the wind speed range 8.6–10.7 and 11.8–13.9 m s^{-1}. (These figures are scaled for a 3-m anemometer height for consistency with our own observations.) Glotov *et al.* (1962) and Blanchard and Woodcock (1957), using a bubble trap technique, also find the bubble density increases rapidly with wind speed.

Knowledge of the behavior of bubble clouds, as well as some of their implications for gas transfer, has also benefited from the remarkable sonar observations by Thorpe and his co-workers (cf. Thorpe *et al.*, 1982; Thorpe, 1982; Thorpe and Hall, 1983). Although their use of a single frequency (248 kHz) does not permit resolution of bubble size distributions, many features of the generation of the bubble clouds, their dependence on convective stability and their spatial and temporal variability were observed. The cloud thickness was observed to take only a few minutes to adjust to a sudden increase in wind speed.

Devin (1959), Medwin (1977a) and Clay and Medwin (1977) give comprehensive surveys of the theory of sound scattering and absorption by clean bubbles. For bubbles much smaller than the acoustic wavelength, the effect can be dominated by bubbles with resonant frequency the same as that of the transmitted sound, although contributions from the tails of the

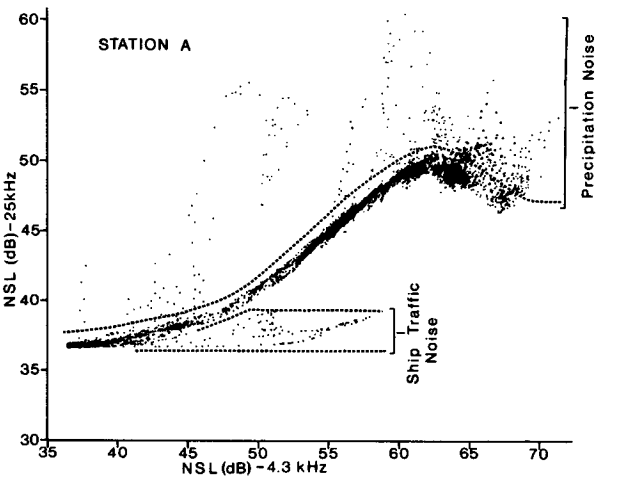

FIG. 8. NSL for 25.0 vs 4.3 kHz for Station A, Series 4, illustrating the effects of rainfall and ship traffic contributions to the noise level. Points lying below the principal curve contain more low-frequency noise, consistent with observed effects due to passing ships. Precipitation noise appears to have significant higher-frequency components and accounts for points lying above the principal curve.

TABLE 3. Radius of resonant bubbles (μm) for different frequencies and depths, corrected for surface tension and nonadiabatic effects.

Depth (m)	Frequency (KHz) 4.3	8.0	14.5	25.0
0	742.0	397.0	217.8	125.5
1	779.2	417.1	228.9	132.0
2	814.7	436.2	239.5	138.2
3	848.7	454.5	249.7	144.1
5	914.0	489.1	268.8	155.2

resonance curve will depend upon bubble size distribution and in general cannot be neglected (see Medwin, 1977b). The resonant frequency and the scattering and absorption cross sections of a bubble of radius a, depend upon the ambient pressure P, ambient water density ρ_w, surface tension τ at the air–water interface, shear viscosity of water μ, density of enclosed gases ρ_g, ratio of their specific heats γ, their specific heat at constant pressure C_p and their thermal conductivity κ. The radius a of a bubble resonant at frequency ω is defined by the root of the equation (cf. Medwin, 1977a):

$$a = \frac{1}{2\pi\omega}(3\gamma bTP/\rho_w)^{1/2}, \tag{1}$$

where

$$T = 1 + \frac{2\tau}{\rho_w a}\left(1 - \frac{1}{3\gamma b}\right),$$

$$b = (1 + D^2)^{-1}\left[1 + \frac{3(\gamma - 1)}{X}\frac{Y}{Z}\right]^{-1},$$

$$X = a(2\omega\rho_g C_p/\kappa)^{1/2},$$

$$Y = \sinh X - \sin X, \quad Z = \cosh X - \cos X,$$

$$Y' = \sinh X + \sin X$$

$$D = 3(\gamma - 1)\left[\frac{XY' - 2Z}{X^2Z + 3(\gamma - 1)XY}\right].$$

Nonadiabatic and surface-tension effects are minor at the frequencies of interest here; for example at 25 kHz and at a depth of 1 m, they are responsible for a decrease in the radius of resonance of a bubble by 2.7%, thus justifying the usual approximation, $bT \approx 1$. However, as discussed below, nonadiabatic effects, represented by the term D, contribute significantly to the absorption cross section, and for consistency the full expression is used in subsequent calculations. A more significant effect on calculations of resonant radius is that of pressure. At 25 kHz a resonant bubble at 5 m has 1.24 the radius of a bubble resonant at the same frequency at the surface. The following calculations are carried out for a mean bubble depth of 1 m.

The acoustic properties of bubbles may be altered to some extent by surface contamination. However the extent of this effect is at present unknown in the ocean and no attempt will be made to include it here. Table 3 lists values of a for the four frequencies of interest.

Figure 9 shows the position of these resonant bubble radii on the bubble population distribution determined by Johnson and Cooke (1979). It appears that for the observed range of bubble sizes, the 25.0 and 14.5 kHz signals have resonant radii lying within the observed distribution and are thus likely to be influenced by the presence of bubbles; the 8.0 kHz signal has a resonant radius close to the upper end of the size range and the 4.3 kHz signal lies well outside it. The 4.3 kHz signal thus appears appropriate for inferring the wind speed since it is unlikely to be influenced significantly by the bubble layer and indeed this is consistent with the anemometer data in Fig. 2 as well as the historically determined wind–noise relationships.

Acoustic waves travelling through a bubbly medium are attenuated by three mechanisms: radiation loss, damping due to shear viscosity and damping due to thermal conductivity. The attenuation may be expressed in terms of the extinction cross section σ_e,

$$\sigma_e = \sigma_s + \sigma_a, \tag{2}$$

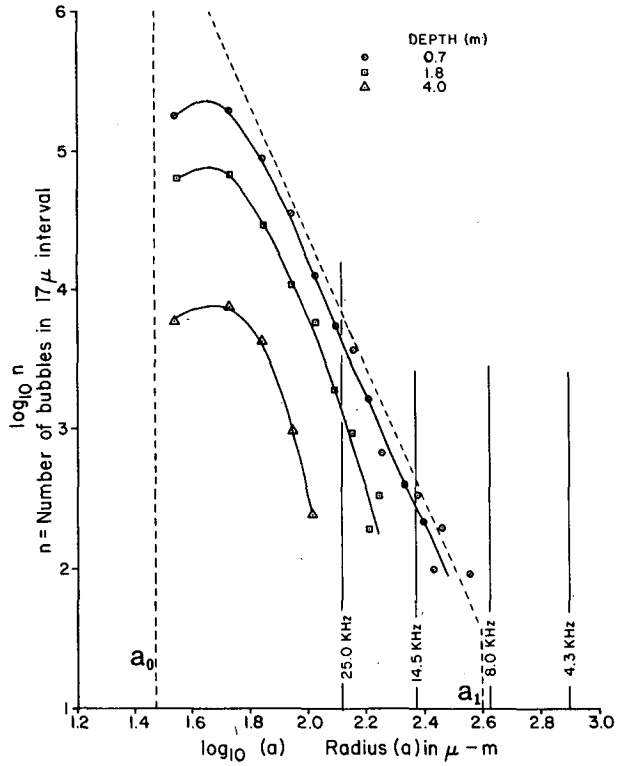

FIG. 9. Plot of photographically determined bubble population, adapted from Johnson and Cooke (1979), showing radii of bubbles resonant at frequencies recorded in Queen Charlotte Sound. Dashed trapezoid represents model bubble population used in calculations; the bubble population density, spectral slope and upper bubble size a_1 are found from the measurements.

where σ_a represents the effects of thermal and viscous losses and σ_s is the scattering cross section at frequency ω (see Medwin 1977a):

$$\sigma_s = \frac{4\pi a^2}{[(\omega_r/\omega)^2 - 1]^2 + \delta^2}, \tag{3}$$

where

$$\delta = ka + D\left(\frac{\omega_r}{\omega}\right)^2 + \frac{4\mu}{\rho_g \omega a^2}$$

is the total damping coefficient (Devin, 1959), and k is the wavenumber. At 25 kHz and 1 m depth, thermal effects account for 0.778, radiation effects for 0.202 and viscous effects for 0.020 of the total extinction.

The total extinction cross section is

$$\sigma_e = \sigma_s(\delta/ka). \tag{4}$$

Values of σ_e and σ_a are plotted for three frequencies in Fig. 10 and values of δ, σ_s and σ_a at resonance are given in Table 3.

At a frequency of 25.0 kHz, 20% of the attenuation due to bubbles along the sound path results from radiation damping. A small proportion of this loss may be compensated by scattering from sound paths that would not otherwise have led to the hydrophone. However, a first-order calculation using a uniform distribution of bubbles over a depth of 1 m and allowing for scattering towards the hydrophone from all possible paths shows this secondary effect to be negligible in the present example and it is neglected in the following calculations.

b. A model for sound attenuation by bubbles

A simple model may be developed for the experimental configuration sketched in Fig. 11. We represent the sound as a uniformly distributed source which is scattered and attenuated by a relatively thin layer of bubbles. The sound is subject to the attenuation expected in bubble-free water and we also allow for the possibility of multiple reflections from the sea floor and surface. There are some obvious limitations to our assumption of horizontal homogeneity in the bubble layer which are briefly discussed later. The effects of interaction between bubbles, which we anticipate are small, are not included; nor do we allow for the effects of dispersion or refraction within the bubble layer, since these will only be significant along grazing ray paths, which are severely attenuated at the higher frequencies of interest here, and which have negligible contribution to the total signal received. In this sense the problem is quite different from more typical sound ranging and propagation studies in which the grazing ray paths are often those of prime interest. As discussed earlier (see Fig. 4), the influence of refraction on the effective listening area is minor, especially at the higher frequencies, for sound speed profiles typical of winter conditions. While there is some uncertainty as to the shape of the radiation pattern of wind generated noise at those frequencies, available data appear to fit a dipole source distribution reasonably well (cf. Urick, 1983; McConnell, 1983). As discussed later, the bubbles themselves will also contribute to the directionality of the signal.

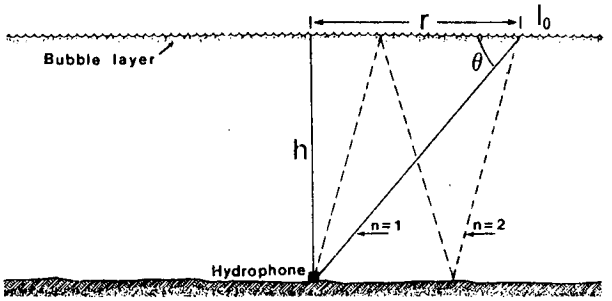

FIG. 11. Experimental configuration and notation used in model of scattering and absorption of wind-generated noise by a thin layer of bubbles. Refraction of the sound is neglected, since at the higher frequencies little of the sound is contributed from shallow angles (see Fig. 4). Solid lines (n = 1) indicate the direct path, dashed lines indicate the first multiple reflection (n = 2).

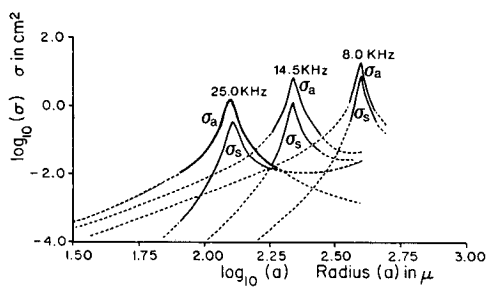

FIG. 10. Attenuation cross section for absorption (σ_a) and radiation (σ_s) loss as a function of bubble radius, for 25.0, 14.5 and 8.0 kHz. Peaks occur at the radius of resonance. The cross sections were determined using expressions given by Devin (1959).

The contribution to the signal received by a hydrophone at depth h, due to a surface sound source of intensity I at radius r, will depend on the attenuation resulting both from absorption and from spreading losses throughout the water column, as well as from absorption and scattering in the surface bubble layer. Attenuation through the bulk of the water column will be a function of the total path length, which is $(h^2 + r^2)^{1/2}$ in the absence of reflection and of refraction effects; attenuation through the relatively thin bubble layer will be a function of the transmission angle θ and of the bubble population density and size distribution. In the case of a dipole radiation pattern, the strength of the source will also be a function of transmission angle,

$$I = I_0 \sin^2\theta.$$

Consider first the unreflected signal from such a dipole point source at radius r in the absence of a

bubble layer. The signal I_r received at the hydrophone, subject only to the effects of spherical spreading and attenuation, will be

$$I_r = I_0 \sin^2\theta(h^2 + r^2)^{-1} \exp[-\alpha(h^2 + r^2)^{1/2}], \quad (5)$$

where α is the attenuation factor for bubble-free water. The presence of a bubble layer results in a second exponential term β, related to the extinction cross section for bubbles given by (4) and subject to a geometrical dependence on the transmission angle:

$$I_r = I_0 \sin^2\theta(h^2 + r^2)^{-1} \exp[-\alpha(h^2 + r^2)^{1/2} - \beta/\sin\theta]. \quad (6)$$

Integration over the ocean surface for a uniformly distributed source yields the signal intensity at the hydrophone, $\bar{I}_r$ due to unreflected sound originating at the surface:

$$\bar{I}_r = \int_0^\infty 2\pi r I_0 \sin^2\theta(h^2 + r^2)^{-1} \exp[-\alpha(h^2 + r^2)^{1/2} - \beta/\sin\theta]dr$$

$$= 2\pi I_0 \int_1^\infty s^{-3} \exp[-(\alpha h + \beta)s]ds$$

$$= 2\pi I_0 E_3(\alpha h + \beta), \quad (7)$$

where E_3 is the exponential integral function of third order and we have used the substitution $s = \csc\theta$. For a monopole radiation pattern the result is identical except that the integral function is of first order. The result for both cases is plotted in Fig. 12. Note that for a monopole source pattern ($i = 1$), the integral is singular in the absence of attenuation; however even if attenuation were negligible, other effects such as refraction, boundary scattering and reflection would render the model invalid in the limit. For a dipole pattern consistent with previously observed wind-noise radiation, the integral is finite even in the absence of attenuation. As the attenuation factors increase, the signal strength at the hydrophone decreases. Dashed lines indicate the attenuation at 14.5 and 25.0 kHz in the absence of bubbles, for the hydrophone depth corresponding to Station A.

There will also be contributions to the received signal from noise that has suffered multiple reflection (and scattering) from the sea floor and surface. Consider reflection coefficients s_1, s_2 for the surface and bottom respectively, that are independent of the intersection angle. Then for multiple reflections we can generalize the solution (7) to

$$\bar{I}_r = 2\pi I_0 \sum_{n=1}^{\infty} (s_1 s_2)^{n-1}(2n - 1)^{-2} E_3[(2n - 1)(\alpha h + \beta)], \quad (8)$$

the first term of which corresponds to the direct path, the second to one pair of reflections and so on. We

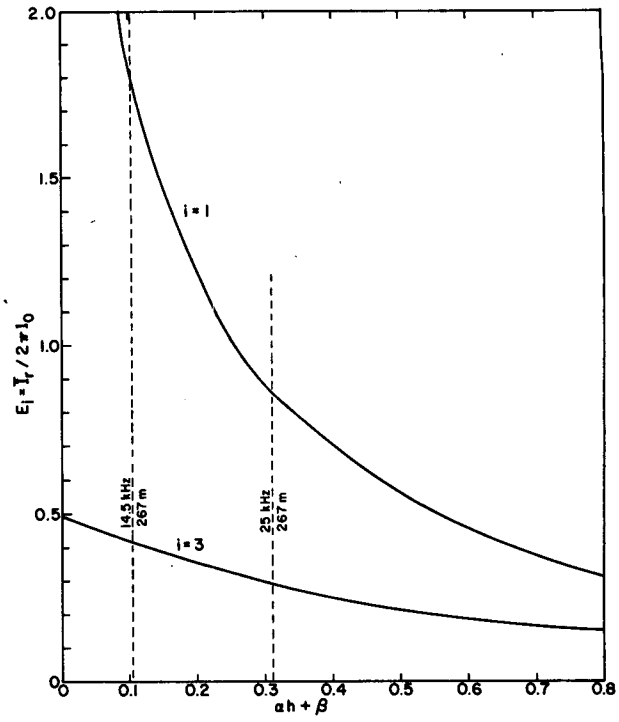

FIG. 12. The model solution (7) of received signal intensity as a function of the attenuation factors ($\alpha h + \beta$), plotted for both monopole and dipole radiation patterns. Dashed lines indicate the argument in the absence of attenuation by a bubble layer for two frequencies at Station A.

determine an upper bound to the contribution of reflected sound by noting that in the absence of any attenuation in the water column or by bubbles ($\alpha h + \beta = 0$) and assuming zero reflection losses at the sea floor and surface ($s_1 = s_2 = 1$), (8) can be summed to yield

$$\bar{I}_r = (\pi^3/8)I_0$$

which is $\pi^2/8$ or 1.23 times the noise level received without reflection. Inclusion of realistic reflection coefficients (i.e., $s_2 \approx 0.1$ for the layered sediments of Queen Charlotte Sound) and of appropriate attenuation losses (see Table 3), shows that actual contributions of reflected sound will be very small. For example, the contribution of the first multiple ($n = 2$), even in the absence of bubble attenuation, surface scattering and surface reflection losses, will be only about 0.003 that of the direct-path noise levels at 14.5 kHz and 0.001 at 25.0 kHz. Thus in the subsequent discussion we take only the first term in the expansion, given by (7).

c. *Model results*

The model solution (7), together with the attenuation characteristics for bubbles (4), provide a basis for explaining departures of the received signal from the spectral characteristics observed at lower wind

speeds. Straight lines of unit slope fitted to the linear parts of the observed data are shown in Fig. 7. For each data point we now find the deviation Δ from the linear extrapolation, as a function of wind speed (or NSL at 4.3 kHz) and of listening frequency. Consistent with our hypothesis that the deviation results from attenuation by bubbles, we relate Δ to the ratio of inferred signal intensities with and without the surface bubble layer,

$$\Delta = 10 \log_{10}[E_3(\alpha h + \beta)/E_3(\alpha h)], \quad \Delta \geq 0, \quad (9)$$

where Δ is expressed in decibels.

For each deviation $\Delta(\omega_0, \omega_i)$ based on the frequency pair ω_0, ω_i, where $\omega_0 = 4.3$ kHz, we may solve (9) to find β. We take the attenuation factor α as a constant for each frequency (see Table 3) at a mean water temperature of 8°C. The exponential integral function is evaluated from a series expansion (Abramowitz and Stegun, 1968, Section 5.1.12) and the corresponding value of β is recovered from (9) by the method of *regula falsi*.

Bubble attenuation factors calculated in this way, for each observed deviation and for frequencies ω_i = 8.0, 14.5 and 25.0 kHz, are plotted in Fig. 13. Both the 14.5 and 25.0 kHz plots illustrate the onset of attenuation at about 10 m s^{-1}, rising steeply thereafter. At 25.0 kHz the bubble attenuation rises more steeply than at 14.5 kHz and there is some scatter in the points, especially at higher wind speeds; at 8.0 kHz the change is more gradual. Some of the scatter in estimates of β may be a consequence of precipitation. Rainfall noise, by contributing more to the higher frequencies, tends to offset the apparent attenuation and reduce the calculated values of β. In the following calculations all available points are used, except for the few for which $\Delta < 0$ and hence β is undefined.

The bubble attenuation factor β_1 at frequency ω_1 is related to the combined scattering and absorption cross section σ_{e_1} (Eq. 4), integrated over the bubble population:

$$\beta_1 = \int_0^\infty N(a)\sigma_{e_1} da \quad (10)$$

In Eq. (10), $N(a)$ is the number of bubbles in radius increment da, centered at a, per unit surface area, integrated over the depth of the bubble layer. Consistent with observed population distributions of Johnson and Cooke (1979) and Kolovayev (1976), we model the bubble population density with a power-law dependence:

$$\left.\begin{aligned} N(a) &= Ka^{-p}, \quad a_0 \leq a \leq a_1 \\ &= 0, \quad a_0 > a > a_1 \end{aligned}\right\}, \quad (11)$$

where K and p may be some function of the wind speed. This distribution is sketched in Fig. 9.

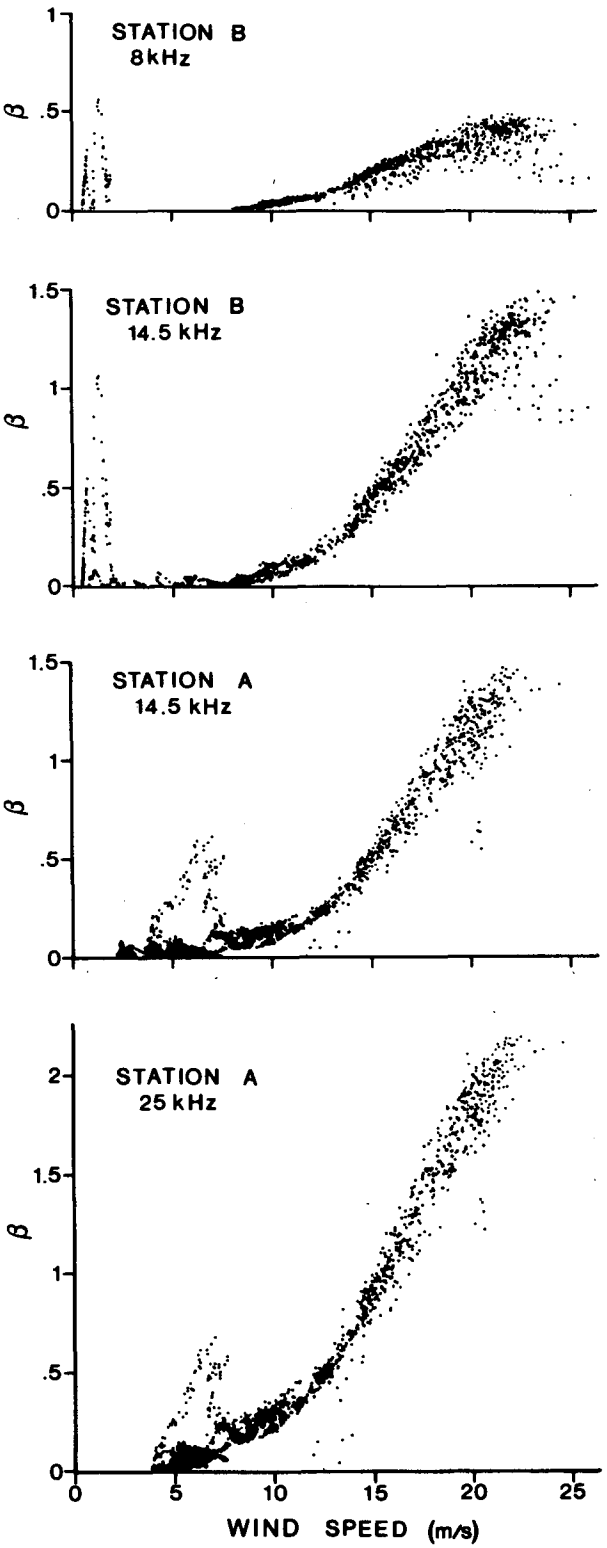

FIG. 13. Bubble attenuation coefficients β for frequencies 8.0, 14.5 and 25.0 kHz determined from Eq. (9) at each station and plotted as a function of wind speed inferred from the 4.3 kHz NSL.

The exponent p is implicitly defined by the ratio of observed bubble attenuation factors β_1/β_2 at two frequencies ω_1, ω_2 lying within the bubble size limits a_0, a_1. From (10) and (11):

$$\beta_1/\beta_2 = \frac{\int_{a_0}^{a_1} a^{-p}\sigma_{e_1} da}{\int_{a_0}^{a_1} a^{-p}\sigma_{e_2} da}. \tag{12}$$

The population density $N(a_i)$ may be found from the ratio between β_i and the corresponding coefficient β_i' for the same distribution function (11), but having unit population density at radius a_i:

$$N(a_i) = \beta_i/\beta_i' \tag{13}$$

$$= \frac{\beta_i}{\int_{a_0}^{a_1} (a/a_i)^{-p}\sigma_e da}.$$

The integrations in (12) were carried out using 2000 points over two bubble size ranges (30–200 μm and 20–400 μm) for $2 \leqslant p \leqslant 7$ in steps of 0.2, with p being evaluated as a function of frequency and bubble radius from the expressions given above. A measure of the relative insensitivity of the integration to the choice of integration limits for the two higher frequencies was determined by comparison of the values calculated using the smaller and the larger ranges; at 14.5 and 25.0 kHz the integrals changed by a maximum of 1.9% and 0.09% for changes in the lower and upper integration bounds respectively. This insensitivity arises from the high Q of bubbles (14–17 at these frequencies) and avoids the necessity of using a more detailed model than (11) for the bubble distribution at small radii; such a simplification would not necessarily apply at higher frequencies. The situation is quite different at 8.0 kHz, since in this case the resonant radius lies close to the presumed outer limit of the bubble distribution (see Fig. 9). Thus we use the two higher frequencies to infer the bubble-size exponent p and we use the 8.0 kHz signal to probe the upper bubble-size limit a_1.

The relationship between the calculated ratio β (25.0 kHz)/β (14.5 kHz) and the exponent p is shown in Fig. 14a. For each observed ratio the corresponding value of p is determined by interpolation of the numerical integrations; the results are plotted in Fig. 14b for wind speeds greater than 10 m s^{-1}. Values decline from a maximum of $p = 4.75$ toward smaller values at higher wind speeds. For comparison we also show corresponding estimates of Kolovayev (1976) and of Johnson and Cooke (1979).

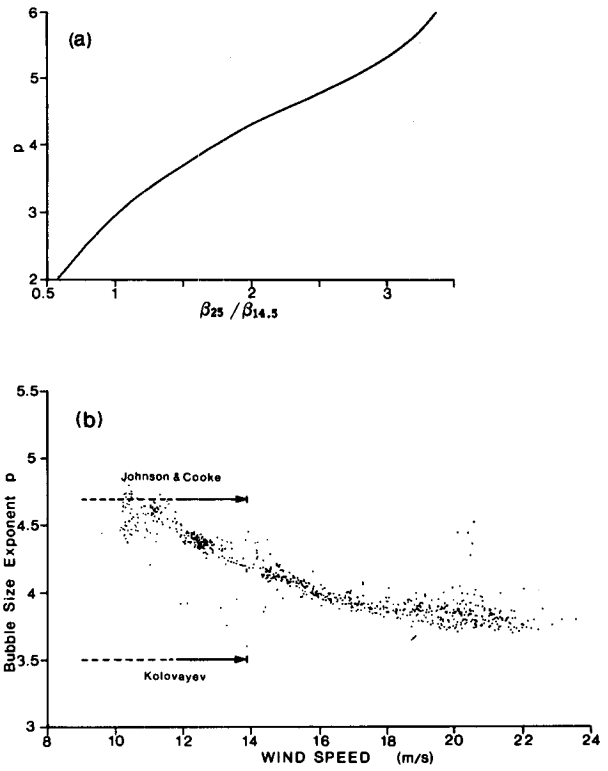

FIG. 14. (a) The relationship between the bubble size exponent p and the ratio of bubble attenuation coefficients at 25.0 and 14.5 kHz, derived from numerical integration of (12). (b) Inferred values of the bubble-size exponent p using bubble attenuation factors for Station A (i.e., Fig. 13) and the numerical relationship shown in Fig. 14(a).

Having established the exponent p in (13), we may now use (12), together with our 8.0 kHz data from Station B, to infer the upper bubble-size limit a_1. Figure 15a shows the relationship between the calculated ratio β (14.5 kHz)/β (8.0 kHz) and a_1. Individually observed ratios and corresponding values of a_1 are plotted as a function of wind speed in Fig. 15b. The results imply a slight decrease in a_1 from about 430 μm at 10 m s^{-1} to about 410 μm at higher speeds. However, we do not expect that the actual distribution will be quite as simple near the outer limits as implied by (11). Moreover the lower attenuation factor applicable at this frequency weakens the basis for our neglect of refraction effects (see Fig. 4). Instead, the results should be interpreted as implying that the size of the largest bubbles contributing significantly to attenuation is of the same order as that resonant at 8.0 kHz (417 μm).

For bubbles of radius resonant at 25.0 or 14.5 kHz we calculate the bubble population density N from (13), using previously determined values of p and a_1. (The lower bubble size in these calculations was set at 30 μm). In Fig. 16 we plot log$N$ against logu_* for

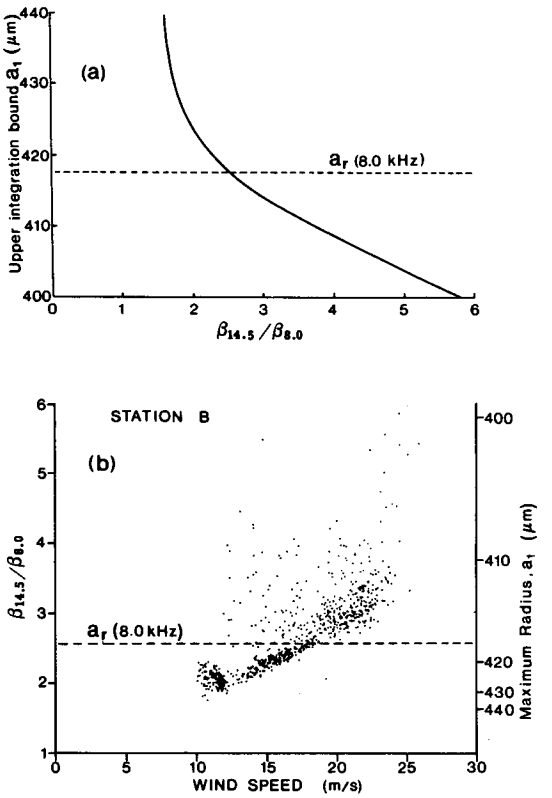

FIG. 15. (a) The relationship between the upper integration bound a_l and the ratio of bubble attenuation coefficients, found by numerical integration of (12). Dashed line shows bubble radius resonant at 8.0 kHz. (b) Inferred upper integration bound determined from the functional relationship shown in (a) and observed values of the ratio $\beta(14.5)/\beta(8.0)$ for Station B.

each frequency. A vertical integration, assuming an exponential depth dependence, of Johnson and Cooke's (1979) values is included for comparison; the friction velocity u_* is calculated for neutral stability since this condition holds for the higher wind speed data set we have used (see Fig. 5b for the period following 1800 h on November 24). Our estimate is rather lower than theirs in the mean for each case although overlapping their values at the upper limit of their observed wind speed for both radii. Johnson and Cooke's estimate for the larger bubbles (229 μm) is close to the limit of their observation range so that their results are subject to substantial (though undetermined) uncertainty. Again we limit our data to wind speeds greater than or equal to 10 m s^{-1}; below this speed, variance greatly increases and no clear-cut pattern emerges.

Kanwisher (1963) estimated that the bubble volume increases more rapidly than wind speed squared which is certainly consistent with our results. Thorpe (1982) found an exponential dependence on wind speed. Kerman (1982) used an extension of Crowther's (1980) theoretical model to infer a u_*^3 dependence. Comparison with these results is complicated by their reference to bubble population densities at a given depth, whereas our inferred populations are integrated over the total bubble-layer thickness. However we note that for $10 < W < 16$ m s^{-1} the slope is about 3 comparable to the theoretical prediction of Kerman (1982); for higher speeds the points fall close to a line of progressively decreasing slope, implying a departure from a power-law dependence on wind speed.

The bubble layer will not only modify the intensity of high-frequency wind-generated noise, but also its directionality. We have already noted that the dependence of attenuation on the angle of transmission reduces the contribution from shallow sound paths. The implications of this effect are seen in the modification of the directivity index of the received signal, defined as

$$D_i = 10 \log_{10}\left(4\pi r^2 I_h \Big/ \int_s I_r ds\right), \qquad (14)$$

where the integration of received signal intensity I_r is carried out over a sphere and the reference intensity I_h is that received from a point immediately overhead. Since our hydrophone is bottom mounted, contributions only arise from points above the horizontal plane that passes through it. Insertion of (6) and (7) into (14) leads to

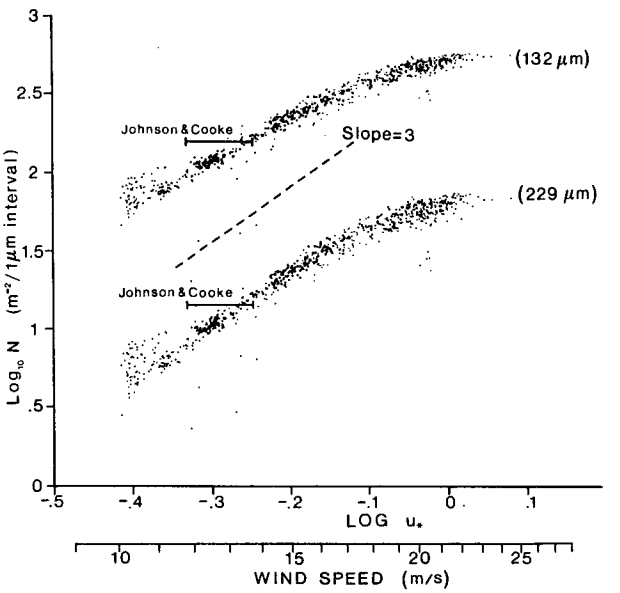

FIG. 16. Inferred bubble population density, vertically integrated over the bubble layer and expressed as a function of the friction velocity u_*, for radii corresponding to resonance at 25.0 and 14.5 kHz. Horizontal bars correspond to values inferred from the distributions found by Johnson and Cooke (1979).

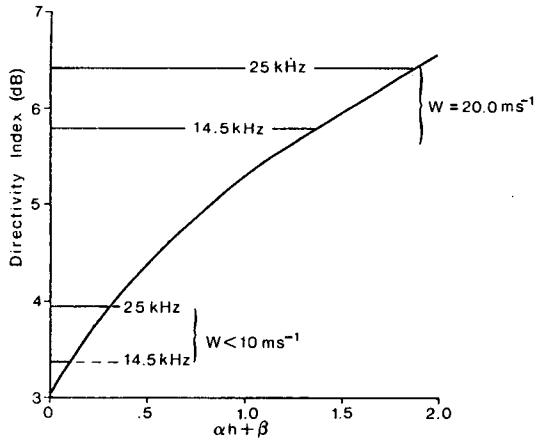

FIG. 17. The directivity index of wind-generated noise received by an omnidirectional hydrophone on the sea floor, expressed as a function of the attenuation factor $\alpha h + \beta$. The curve is plotted for a dipole radiation pattern, and illustrates the increase in directivity resulting from the angular dependence of attenuation on the bubble layer. The effect increases with wind speed and with acoustic frequency.

$$D_i = -10 \log_{10}[\exp(\alpha h + \beta) E_3(\alpha h + \beta)], \quad (15)$$

which is plotted in Fig. 17. For wind speeds less than 10 m s^{-1} only minor differences in directionality occur between the two higher frequencies. The signal is much more directional at higher wind speeds and the effect is greater at the higher frequency.

5. Conclusions

Ambient noise measurements obtained at depths of ~260 m off the British Columbia coast have provided new evidence of the effects of bubbles near the ocean surface. At wind speeds greater than about 10 m s^{-1}, wind-generated noise measured at 14.5 and 25.0 kHz appears to be attenuated by an amount that increases with wind speed and is greater at the higher acoustic frequency. Smaller but still significant effects were also observed at 8.0 kHz. At 4.3 kHz the noise spectrum levels were found consistent with available wind speed data from a nearby lightstation, using an empirical relationship derived from similar measurements at the same location the previous summer.

A model is developed that explains the apparent attenuation of the noise generated at the ocean surface at high wind speeds, as a consequence of scattering and absorption by the thin layer of bubbles produced by breaking waves. Conversely, the model allows inversion of the inferred attenuation to determine the properties and behavior of the bubble layer itself. The inversion is based on the assumption that the linear relationship between the signal intensity at different frequencies, which is clearly observed at wind speeds of 2–10 m s^{-1}, is also representative of the sound generated at higher wind speeds and that departures from this linear relationship are a consequence of the bubble layer.

A test of the validity of this assumption lies in the consistency of our inferred bubble populations with those determined by independent measurement. Unfortunately such independent measurements are sparse and only representative of populations at discrete depths, thus complicating comparisons with our vertically integrated values. Nevertheless, the results of this study are not inconsistent with previous measurements. Our inferred size distribution parameter, $p = 4.75 - 3.75$, is close to Johnson and Cooke's (1979) value of 4.7 at lower speeds, declining at higher speeds. The inferred population density is near, although less than the range observed by Johnson and Cooke, and changes rapidly at wind speeds applicable to their data. The upper limit of bubble size (417 μm) that we observed is slightly larger than the largest bubbles seen by Johnson and Cooke, but this is to be expected, given the low density of such bubbles and the small volume used for photographic observation. Notwithstanding the difficulty of comparison, we thus find that these independent observations are generally consistent with our own and tend to support the validity of the assumptions underlying the inversion.

It is certain that our assumption of a horizontally uniform bubble distribution and a horizontally homogeneous noise source is inadequate at lower wind speeds. If, as Kerman (1984) proposes, the noise is generated by bubble shattering within the whitecaps, it will be discretely distributed both in space and time. The whitecaps are also the source of the bubbles that are responsible for attenuation of the sound. However injection of the bubbles into the surface layer by the moving whitecaps results in elongated trails of bubbles (Thorpe and Hall, 1983). Thus at lower wind speeds the bubble layer is patchy, and the probability of a whitecap occurring above a bubble cloud is reduced. This feature will account for the absence of noticeable attenuation at low wind speeds (5 m s^{-1}) even though whitecaps, and hence the bubble clouds, are known to occur. At higher wind speeds the clouds of bubbles will tend to overlap forming a continuous layer (Thorpe, 1982). However the bubble-layer thickness remains variable at these higher wind speeds and this variability will lead to variability in the attenuation, which will contribute to the scatter observed in our data. Similar scatter at higher wind speeds was also noted by Wille and Geyer (1984).

The bubble population at higher wind speeds is relevant to the problem of gas flux across the air–sea

interface. Merlivat and Memery (1983) have demonstrated the rapid increase in gas exchange that occurs with the onset of breaking waves and injection of bubbles into the surface layer. Thorpe (1982) showed that the flux through bubbles is significant at 12 m s^{-1}, but as he points out, more needs to be known about the variation of bubble populations at higher wind speeds, especially in the open sea. The present study, carried out in an exposed area on the edge of the continental shelf with unrestricted fetch from the west and south, shows that the population continues to rise with increasing wind speed, though not as steeply as it does at lower wind speeds. Further studies, both of the bubbles and of the ambient noise field as well as of the influence of surface contamination on the acoustic properties of bubbles will undoubtedly lead to refinement of the estimates of the bubble size distribution and population density for different meteorological and oceanographic conditions. However such refinements are unlikely to alter the basic result of this study, that bubbles entrained by breaking waves provide acoustic insulation and at high wind speed and high acoustic frequencies they can account for the observed decrease in ambient noise level.

Modification of the ambient noise field by the surface bubble layer will also have implications for acoustic remote sensing of wind speed and precipitation. It appears that frequencies well below 8 kHz should be used if unbiased estimates of wind speed above 10 m s^{-1} are to be obtained from ambient noise measurements. The noise produced by falling rain is thought to have a spectral peak between 15 and 20 kHz (J. Nystuen, personal communication, 1983); this signal also will be influenced by the bubble clouds. The present study has drawn attention to one aspect of high-frequency ambient noise in the ocean, but it is clear that much remains to be learned about the physical processes underlying its generation, intensity, variability and radiation pattern, especially at higher wind speeds. Investigation of these natural sound sources, coupled with the use of appropriate active sounding techniques, appears to be a useful approach to the study of the complex behavior characterizing the boundary between atmosphere and ocean.

Note added in proof: Recent work by Thorpe (1984a,b) has drawn attention to the influence of Langmuir circulation on bubbles, and provides at least one reason why we should expect Johnson and Cooke's (1979) measurements to lead to overestimates of the mean bubble population.

Acknowledgment. Dr. A. D. Booth provided valuable assistance with numerical analysis. We are indebted to G. Kamitakahara-King for carrying out the data processing and plotting. The integrations in Fig. 4 were carried out by S. Vagle. Wave data were kindly provided by B. de Lange Boom of Seakem Oceanography; the CTD profiles in Fig. 3 were provided by Dr. S. Tabata. Deployment and recovery of the instruments was carried out by the Coastal Zone Oceanography group at IOS.

REFERENCES

Abramowitz, M. A., and I. A. Stegun, 1968: *Handbook of Mathematical Functions,* Dover, 1046 pp.

Blanchard, D. C., and A. H. Woodcock, 1957: Bubble formation and modification in the sea and its meteorological significance. *Tellus,* **9,** 145–158.

Clay, C. S., and H. Medwin, 1977: *Acoustical Oceanography; Principles and Applications.* Wiley & Sons, 541 pp.

Crowther, P. A., 1980: Acoustical scattering from near-surface bubble layers. *Cavitation and Inhomogeneities in Underwater Acoustics,* W. Lauterborn, Ed., Springer-Verlag, 194–204.

Devin, C., Jr., 1959: Survey of thermal, radiation and viscous damping of pulsating bubbles. *J. Acoust. Soc. Amer.,* **31,** 1654–1667.

Evans, D. L., and D. R. Watts, 1982: Wind speed and stress at the sea surface from ambient noise measurements. *Proc. Int. Symp. Acoustics Remote Sensing Atmos. and Oceans.,* Dept. Physics, University of Calgary, Calgary, Canada, III69–III78 pp.

Glotov, V. P., P. A. Kolobaev, and G. G. Neuimin, 1962: Investigation of scattering of sound by bubbles generated by an artificial wind in sea water and the statistical distribution of bubble sizes. *Sov. Phys. Acoust.,* **7,** 341–345.

Hill, W., 1984: A generation of WOTAV underwater wind-recording instruments, *Proc. IEEE, OCEANS '84,* 31–36.

Johnson, B. D., and R. C. Cooke, 1979: Bubble population and spectra in coastal waters: a photographic approach. *J. Geophys. Res.,* **84,** 3761–3766.

Kanwisher, J., 1963: On the exchange of gases between the atmosphere and the sea. *Deep-Sea Res.* **10,** 195–207.

Kerman, B. R., 1982: Distribution of bubbles near the ocean surface. Rep. AQRB-82-008-L, Boundary Layer Res. Div. Atmos. Environ. Serv., Downsview, Canada, 21 pp.

——, 1984: Underwater sound generation by breaking wind waves. *J. Acoust. Soc. Amer.,* **75,** 149–165.

Kerman, B. R., D. L. Evans, D. R. Watts and D. Halpern, 1983: Wind dependence of underwater ambient noise. *Bound. Layer Meteor.,* **26,** 105–113.

Knudsen, V. O., R. S. Alford, and J. W. Emling, 1948: Underwater ambient noise. *J. Mar. Res.* **7,** 410–429.

Kolovayev, D. A., 1976: Investigation of the concentration and statistical size distribution of wind-produced bubbles in the near surface ocean. *Oceanol.,* **15,** 659–661.

Lemon, D. D., D. M. Farmer and D. R. Watts, 1984: Acoustic measurements of wind speed and precipitation over a continental shelf. *J. Geophys. Res.,* **89,** 3462–3472.

McConnell, S. O., 1983: Remote Sensing of the air–sea interface using microwave acoustics. *Proc. IEEE, OCEANS '83,* 1–8.

Medwin, H., 1977a: Counting bubbles acoustically: A review. *Ultrasonics,* **15,** 7–13.

——, 1977b: Acoustical determination of bubble-size-spectra. *J. Acoust. Soc. Amer.,* **62,** 1041–1044.

Merlivat, L., and L. Memery, 1983: Gas exchange across an air–

water interface: experimental results and modeling of bubble contribution to transfer. *J. Geophys. Res.*, **88,** 707–724.

Perrone, A. J., 1969: Deep ocean ambient noise spectra in the northwest Atlantic. *J. Acoust. Soc. Amer.*, **46,** 762–770.

——, 1970: Ambient-noise-spectrum levels as a function of water depth. *J. Acoust. Soc. Amer.*, **48**(Part 2), 362–370.

Shaw, P. T., D. R. Watts, and H. T. Rossby, 1978: On the estimation of oceanic wind speed and stress from ambient noise measurements. *Deep-Sea Res.*, **25,** 1225–1233.

Thorpe, S. A., 1982: On the clouds of bubbles formed by breaking waves in deep water and their role in air–sea gas transfer. *Phil. Trans. Roy. Soc. London,* **A304,** 155–210.

——, and A. J. Hall, 1983: The characteristics of breaking waves, bubble clouds, and near-surface currents observed using side-scan sonar. *Cont. Shelf Res.*, **1,** 353–384.

——, A. R. Stubbs and A. J. Hall, 1982: Wave produced bubbles observed by side-scan sonar. *Nature,* **296**(No. 5858), 636–638.

——, 1984a: The effect of Langmuir circulation on the distribution of submerged bubbles caused by breaking wind waves. *J. Fluid Mech.*, **142,** 151–170.

——, 1984b: A model of the turbulent diffusion of bubbles below the sea surface. *J. Phys. Oceanogr.*, **14,** 841–854.

Urick, R. J., 1983: *Principles of Underwater Sound,* third ed. McGraw-Hill, 423 ppp.

Wenz, G. M., 1962: Acoustic ambient noise in the ocean: Spectra and sources. *J. Acoust. Soc. Amer.*, **34,** 1936–1956.

Wille, P. C., and D. Geyer, 1984: Measurements on the origin of the wind-dependent ambient noise variability in shallow water. *J. Acoust. Soc. Amer.* **75**(1), 173–185.

Wilson, J. H., 1980: Low frequency wind-generated noise produced by the impact of spray with the ocean's surface. *J. Acoust. Soc. Amer.*, **68,** 952–956.

Wu, J., 1981: Bubble populations and spectra in near-surface ocean: summary and review of field measurements. *J. Geophys. Res.*, **86,** 457–463.